

PCCP

Accepted Manuscript



This is an *Accepted Manuscript*, which has been through the Royal Society of Chemistry peer review process and has been accepted for publication.

Accepted Manuscripts are published online shortly after acceptance, before technical editing, formatting and proof reading. Using this free service, authors can make their results available to the community, in citable form, before we publish the edited article. We will replace this *Accepted Manuscript* with the edited and formatted *Advance Article* as soon as it is available.

You can find more information about *Accepted Manuscripts* in the [Information for Authors](#).

Please note that technical editing may introduce minor changes to the text and/or graphics, which may alter content. The journal's standard [Terms & Conditions](#) and the [Ethical guidelines](#) still apply. In no event shall the Royal Society of Chemistry be held responsible for any errors or omissions in this *Accepted Manuscript* or any consequences arising from the use of any information it contains.

ARTICLE

Properties and reactivities of nonheme iron(IV)-oxo versus iron(V)-oxo: Long-range electron transfer versus hydrogen atom abstraction

Cite this: DOI: 10.1039/x0xx00000x

Received 00th January 2012,
Accepted 00th January 2012

DOI: 10.1039/x0xx00000x

www.rsc.org/

Baharan Karamzadeh,^a Devendra Singh,^b Wonwoo Nam,^{*c} Devesh Kumar^{*b} and Sam P. de Visser^{*a}

Recent work of Nam and co-workers [J. Yoon, S. A. Wilson, Y. K. Jang, M. S. Seo, K. Nehru, B. Hedman, K. O. Hodgson, E. Bill, E. I. Solomon and W. Nam, *Angew. Chem. Int. Ed.*, 2009, **48**, 1257] on a biomimetic iron complex implicated a mixture of iron(IV)-oxo and iron(V)-oxo intermediates but the latter could not be spectroscopically characterized, hence its involvements was postulated. To gain insight into the relative activity of these iron(IV)-oxo versus iron(V)-oxo intermediates, we have performed an extensive density functional theory (DFT) study into the chemical properties of the chemical system of Nam et al, namely $[\text{Fe}(\text{O})(\text{BQEN})(\text{NCCH}_3)]^{2+/3+}$ with BQEN = *N,N'*-dimethyl-*N,N'*-bis(8-quinolyl)ethane-1,2-diamine and their reactivity in hydrogen atom abstraction from ethylbenzene. We show that the perceived iron(V)-oxo species actually is an iron(IV)-oxo ligand cation radical, similar to cytochrome P450 compound I. Moreover, this intermediate has an extremely large electron affinity and therefore can abstract electrons from substrates readily. In our particular system, this means that prior to the hydrogen atom abstraction, an electron is abstracted to form an iron(IV)-oxo species, which subsequently abstracts a hydrogen atom from substrate. Thus, our calculations show for the first time how some nonheme iron complexes react by long-range electron transfer and others directly via hydrogen atom abstraction. We have rationalized our results with detailed thermochemical cycles that explain the observed reactivity patterns.

Introduction

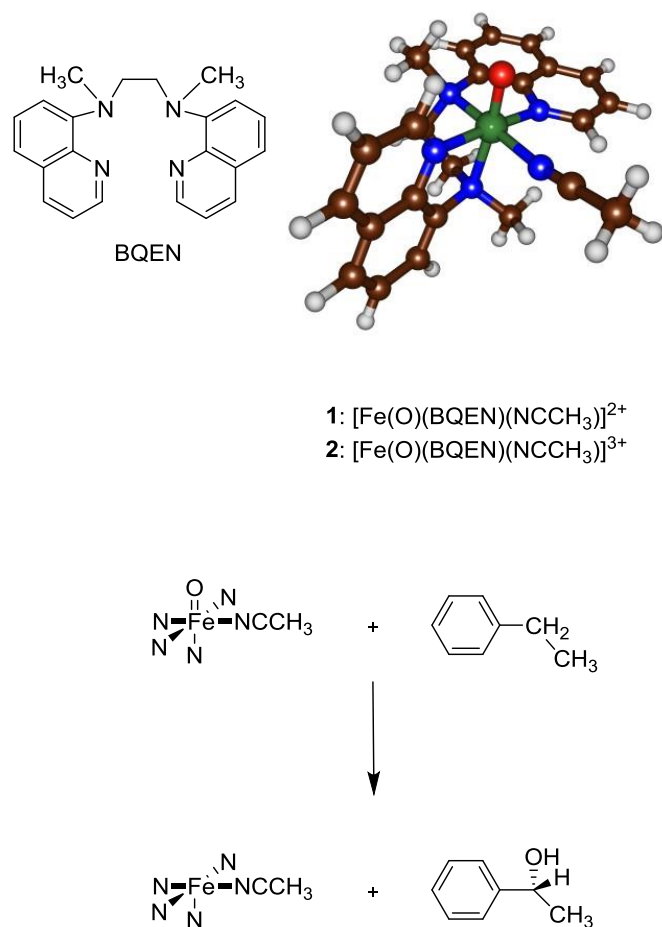
Nonheme iron dioxygenases are important enzymes for human health with essential functions that include DNA base repair mechanisms and oxidative cleavage of carotenoids.¹ In several organisms, natural product biosynthesis is catalysed by nonheme iron dioxygenases, and, therefore, they have important functions in biology as well as in biotechnology. In order to understand enzymatic reaction processes, synthetic model complexes have been developed and designed.² These biomimetic model complexes of nonheme iron oxidants are well studied and many biomimetic high-valent catalytic intermediates have been characterized in recent years.³ For instance, to tackle the controversy in Rieske dioxygenases regarding the active oxidant in the reaction process, several biomimetic model complexes with iron(V)-oxo(hydroxo) as reactive features have been studied and their reactivity patterns established.⁴

All biomimetic Rieske dioxygenase models contain a hydroxo group in a *cis*-position of the iron(IV/V)-oxo group. Only few examples exist of biomimetic iron(V)-oxo intermediates without this *cis*-hydroxo ligand and spectroscopic studies gave indirect evidence of its existence.⁵ Thus, McKenzie and co-workers reported the structural characterization of an iron(V)-oxo species with a monoionic

multidentate ligand and found it to react with thioanisole efficiently.⁶ Kim and co-workers used a tetradentate ligand system and formed the corresponding iron(V)-oxo species by heterolytic cleavage of an iron-acylperoxo intermediate.⁷ They determined kinetic isotope effects (KIE, $k_{\text{H}}/k_{\text{D}}$), H_2^{18}O exchange reactions and measured product distributions. Using a tetraamido macrocyclic ligand, Collins and co-workers studied the sulfoxidation of substrates by an iron(V)-oxo species and compared the rates with analogous iron(IV)-oxo species.⁸ Finally, Nam and co-workers studied the reaction of $[\text{Fe}^{\text{IV}}(\text{BQEN})]^{2+}$, BQEN = *N,N'*-dimethyl-*N,N'*-bis(8-quinolyl)ethane-1,2-diamine, with $\text{CH}_3\text{CO}_3\text{H}$ and found evidence of competing reaction mechanisms originating from two oxidants in the reaction mixture that were tentatively assigned as $[\text{Fe}^{\text{IV}}(\text{O})(\text{BQEN})]^{2+}$ and $[\text{Fe}^{\text{V}}(\text{O})(\text{BQEN})]^{3+}$.⁹ Their studies failed to unequivocally assign the active oxidant in the reaction mechanism, and therefore could not assign the relative reactivity of iron(IV)-oxo versus iron(V)-oxo. In order to resolve this dichotomy and gain general insight into the relative reactivity of iron(IV)-oxo versus iron(V)-oxo with nonheme ligand systems a computational study was conducted using the $[\text{Fe}^{\text{IV}}(\text{O})(\text{BQEN})(\text{NCCH}_3)]^{2+}$ (1) and $[\text{Fe}^{\text{V}}(\text{O})(\text{BQEN})(\text{NCCH}_3)]^{3+}$ (2) systems, Scheme 1.

Currently, very little is known on the catalytic activity of iron(V)-oxo intermediates and to the best of our knowledge, no

direct comparison in reactivity between iron(IV)-oxo and iron(V)-oxo has been reported. We present here a DFT study to gain insight into the potential use of iron(V)-oxo intermediates as catalytic oxidant with ethylbenzene as the selected substrate. We present the first comparative study into the aliphatic hydroxylation by iron(IV)-oxo versus iron(V)-oxo using the BQEN ligand system in Scheme 1 and follow the mechanism of ethylbenzene activation leading to benzyl alcohol product complexes.



Methods

All studies reported here utilize density functional theory (DFT) methods as implemented in the *Jaguar* and *Gaussian* program packages.¹⁰ We initially did exploratory gas-phase optimizations on $[\text{Fe}(\text{O})(\text{BQEN})(\text{NCCH}_3)]^{3+/2+}$ in *Jaguar* at the UB3LYP level of theory¹¹ and explored the catalytic mechanism of ethylbenzene hydroxylation. However, as most of our chemical systems are multiply charged ions we decided to do a subsequent set of calculations, where the complete project was done using a polarized continuum solvent model included during the geometry optimizations. These studies gave considerable differences from the gas-phase results and therefore we will focus on the solvent optimized calculations mainly. Details of the gas-phase calculations can be found in the Electronic Supporting Information. Thus, all geometry optimizations and frequencies were performed with a solvent model included with a dielectric constant mimicking acetonitrile. All local minima are characterized with a

frequency calculation and have real frequencies only, whereas the transition states have one imaginary frequency for the correct mode. As transition metal containing complexes give close-lying electronic and spin states,¹² we calculated the $[\text{Fe}(\text{O})(\text{BQEN})(\text{NCCH}_3)]^{3+}$ complexes in the lowest lying doublet, quartet and sextet spin states and the $[\text{Fe}(\text{O})(\text{BQEN})(\text{NCCH}_3)]^{2+}$ complexes in the singlet, triplet and quintet spin states.

We tested the reproducibility and reliability of the density functional method by applying a range of unrestricted DFT methods, including B3LYP,¹¹ B3LYP-D3,¹³ B3LYP*,¹⁴ and OPBE.¹⁵ There is a certain degree of fluctuation observed in the relative energies, spin state ordering and geometric details as commonly observed in nonheme iron complexes.¹⁶ However, the results confirmed the assignment of the electron configuration of all complexes and reproduce experimental trends.

All optimizations and frequencies use a triple- ζ quality basis set (BS2) with LACV3P+ on iron and 6-311+G* on the rest of the atoms.¹⁷ Previously, we used these methods extensively for the description of nonheme iron complexes and reproduced experimental free energies of activation within several kcal mol⁻¹.¹⁸ To test the effect of the overall charge on the calculations we also performed a set of test calculations to neutralize the reactants and rate determining transition states by adding counter-ions at a fixed distance of 15 Å from the axial nitrogen atom and with an angle of 120 degrees with respect to iron and the axial nitrogen atom. Point charges, Cl⁻ counter-ions and OH⁻ counter-ions were applied, but all results reproduced the solvent optimized results and did not give changes to the charge and spin distributions.

Kinetic isotope effects (KIEs) were calculated for the hydrogen atom abstraction reaction of ethylbenzene by **1** for the replacement of one or more hydrogen atoms of the substrate by deuterium atoms. We initially used the semi-classical Eyring equation (Eq 1) to calculate KIE_E from the difference in free energies of activation (ΔG^\ddagger) of the substrate and its deuterium substituted form following previously reported methods.¹⁹ Eq 1 uses the gas constant (R) and the actual temperature (273.15 K).

$$\text{KIE}_E = k_H/k_D = \exp\{(\Delta G_D^\ddagger - \Delta G_H^\ddagger)/RT\} \quad (1)$$

Further corrections due to tunnelling were applied using the Wigner model²⁰ that corrects KIE_E with the tunnelling ratio (Q_{tH}/Q_{tD}) as described in Eq 2 and 3.

$$\text{KIE}_W = \text{KIE}_E \times Q_{tH}/Q_{tD} \quad (2)$$

$$Q_t = 1 + \frac{1}{24} \left(\frac{h\nu}{k_B T} \right)^2 \quad (3)$$

In Eq 3, k_B represents the Boltzmann's constant, h is Planck's constant and ν is the imaginary frequency in the transition state.

Results

Isolated reactants 1 and 2.

Our study uses density functional theory (DFT) methods and is focused on the chemical systems of Ref 9 as described in Scheme 1, where we included an acetonitrile solvent molecule in the sixth ligand position of the metal: $[\text{Fe}(\text{O})(\text{BQEN})(\text{NCCH}_3)]^{2+}$ (**1**) and $[\text{Fe}(\text{O})(\text{BQEN})(\text{NCCH}_3)]^{3+}$ (**2**). These structures have the metal in formal oxidation state

iron(IV) and iron(V), respectively. Before we will look into the reactivity patterns of structures **1** and **2** with substrates, we will describe the electronic properties of the optimized geometries of **1** and **2**, Fig 1.

The lowest lying singlet, triplet and quintet spin states of **1** were calculated, but the singlet state was found to be high in energy. Similarly, **2** was investigated in the doublet and quartet spin states only. Fig 1 displays the molecular valence orbitals of **1** and **2**, which are determined by the mixing of the metal 3d orbitals with its ligands. Thus, there are three π^* molecular orbitals (π^*_{xy} , π^*_{yz} , π^*_{xz}) representing the anti-bonding interactions of the 3d iron orbitals with 2p orbitals on the oxo group. High in energy are two σ^* orbitals for the anti-bonding interactions of the metal with the ligands in the xy -plane ($\sigma^*_{x^2-y^2}$) and with ligands along the z -axis ($\sigma^*_{z^2}$), whereby the z -axis is defined as parallel to the Fe–O bond. In the iron(IV)-oxo complex, i.e. $^3\mathbf{1}$, the set of orbitals shown in Fig 1 is occupied by four electrons, which gives two low-lying solutions with either triplet or quintet spin: **1** has a triplet spin ground state with electronic configuration $\pi^*_{xy}{}^2 \pi^*_{xz}{}^1 \pi^*_{yz}{}^1$ ($^3\mathbf{1}$) that is somewhat lower in energy than the quintet spin state with configuration $\pi^*_{xy}{}^1 \pi^*_{xz}{}^1 \pi^*_{yz}{}^1 \sigma^*_{x^2-y^2}{}^1$ ($^5\mathbf{1}$), *vide supra*. In both spin states **1** has the metal in formal oxidation state iron(IV). The spin state ordering matches previous studies on

hexacoordinated nonheme iron biomimetic model complexes and also supports the experimentally reported absorption band at $\lambda_{\max} = 740$ nm characteristic for triplet iron(IV)-oxo species and assigned by Nam et al on $[\text{Fe}(\text{O})(\text{BQEN})(\text{NCCH}_3)]^{2+}$.^{3,9,21}

Upon oxidation of $^3\mathbf{1}$, however, several possibilities arise for the electronic configuration of **2**. Firstly, $^3\mathbf{1}$ can lose an electron from π^*_{yz} to give a doublet spin configuration with $\pi^*_{xy}{}^2 \pi^*_{xz}{}^1$ orbital occupation or lose an electron from the doubly occupied π^*_{xy} orbital to give a quartet spin complex with $\pi^*_{xy}{}^1 \pi^*_{xz}{}^1 \pi^*_{yz}{}^1$ configuration. These two states have the metal in formal oxidation state iron(V) and are labelled as $^2\mathbf{2}$ in Fig 1. In addition, the oxidation of $^3\mathbf{1}$ can expel an electron from a ligand π -type orbital, such as π^*_{BQEN} , and lead to an electronic configuration $\pi^*_{xy}{}^2 \pi^*_{xz}{}^1 \pi^*_{yz}{}^1 \pi^*_{\text{BQEN}}{}^1$, whereby the radical on the ligand can be either ferromagnetically or anti-ferromagnetically coupled to the metal-based unpaired electrons in an overall quartet or doublet spin state ($^4\mathbf{2}'$). The latter, therefore, can be seen as an iron(IV)-oxo ligand cation radical species with configuration $[\text{Fe}^{\text{IV}}(\text{O})(\text{BQEN}^+)(\text{NCCH}_3)]^{3+}$ and is reminiscent of Compound I of cytochrome P450 enzymes, which was characterized as an iron(IV)-oxo heme cation radical species, i.e. $[\text{Fe}^{\text{IV}}(\text{O})(\text{heme}^+)\text{Cys}]$.²²

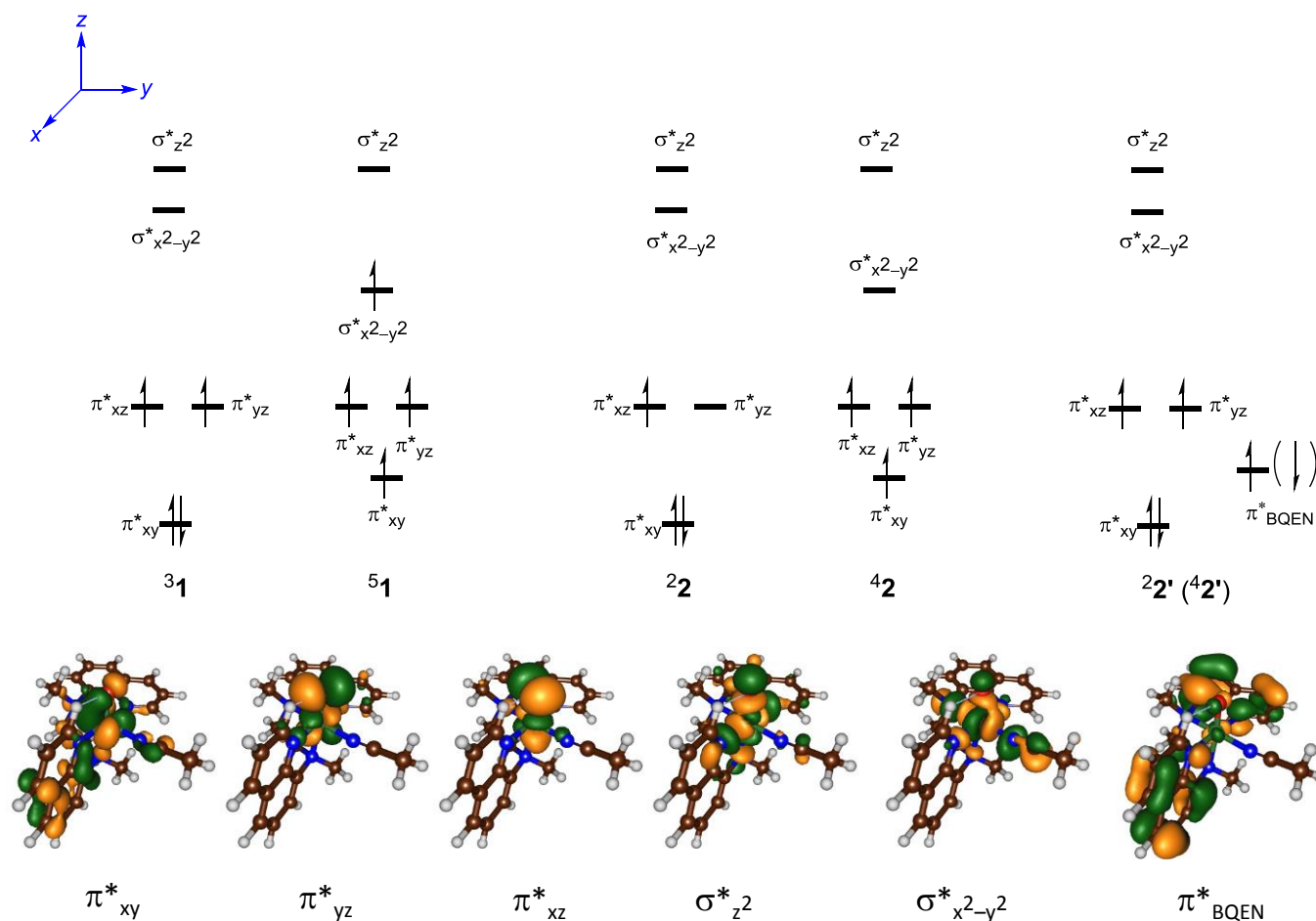


Fig 1. High-lying occupied and low-lying virtual orbitals of **1** and **2**. The top panel gives the different electronic configurations of **1** and **2** considered and the bottom gives the orbital shapes of the valence orbitals.

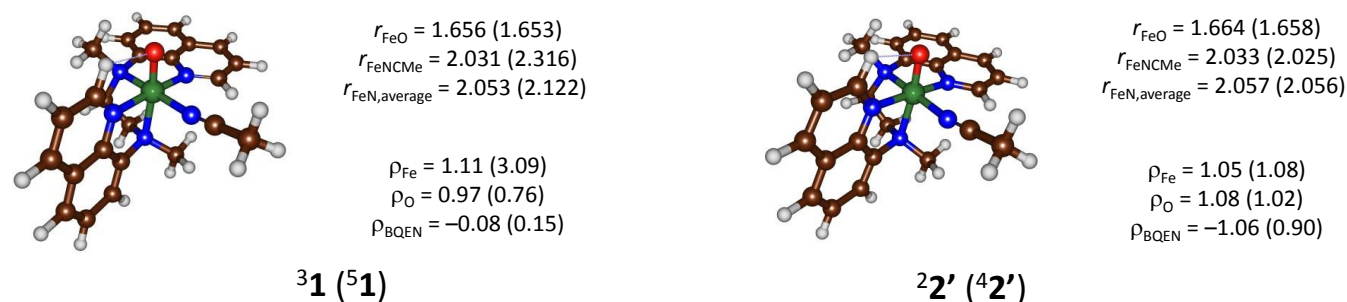


Fig 2. Gas-phase optimized geometries (UB3LYP/BS1) of $^{3,5}\mathbf{1}$ and $^{2,4}\mathbf{2}$ with bond lengths in angstroms and group spin densities (ρ) in atomic units.

Details of the optimized geometries of $^{3,5}\mathbf{1}$ and $^{2,4}\mathbf{2}$ in the gas phase are reported in Fig 2. In the gas-phase the triplet spin state is the ground state by $\Delta E + \text{ZPE}$ (ΔG) = 2.0 (0.2) kcal mol $^{-1}$. Optimized geometries are in line with previously reported structures on non-heme iron(IV)-oxo complexes with a short Fe–O bond of 1.66 Å, which implicates a double bond.^{21,23} Group spin densities and charges confirm the orbital assignment of $^{3,5}\mathbf{1}$ as described in Fig 2 with electronic configuration of $\pi^*_{xy}{}^2 \pi^*_{xz}{}^1 \pi^*_{yz}{}^1$ for $^{3,5}\mathbf{1}$ and $\pi^*_{xy}{}^1 \pi^*_{xz}{}^1 \pi^*_{yz}{}^1 \sigma^*_{x^2-y^2}{}^1$ for 5,1 .

Nam and co-workers⁹ using absorption and infrared spectroscopy and extended X-ray absorption fine structure (EXAFS) studied the [Fe(O)(BQEN)(NCCH₃)²⁺ complex experimentally. They identified an iron-oxo bond of 1.67 Å and an average Fe–N distance of 1.97 Å. Our calculated Fe–O distances for $^{3,5}\mathbf{1}$ in Fig 2 match the experimental values excellently. The experimentally reported Fe–N distances are in good agreement with the triplet spin structures, but not with the quintet spin state structures due to single occupation of the $\sigma^*_{x^2-y^2}$ orbital that elongates the distances between the metal and its ligands. Therefore, the computational studies support the characterization of a triplet spin ground state of $\mathbf{1}$.

Geometry optimizations of $^{2,4}\mathbf{2}$, however, gives a low-lying solution with two singly occupied π^* orbitals coupled to a radical on the BQEN unit with spin densities of $\rho_{\text{BQEN}} = -1.06$ (0.90) in the doublet and quartet spin states. The optimized geometries, therefore, correspond to an electronic state [Fe^{IV}(O)(BQEN⁺)(NCCH₃)³⁺, i.e. $^{2,4}\mathbf{2}$ in Fig 1, rather than an iron(V)-oxo species. Although we attempted to swap molecular orbitals to generate the iron(V) solution ($^{2,4}\mathbf{2}$) these calculations converged back to $^{2,4}\mathbf{2}$, which therefore is the molecular ground state.

As the complex has a large overall charge of +3, we decided to reoptimize these structures using the polarized continuum model mimicking an acetonitrile solution. However, the new model did not affect the spin state ordering and electronic configuration of the ground state and the same electronic state was found. It appears, therefore, that $^{2,4}\mathbf{2}$ is the electronic ground state that can be described as [Fe^{IV}(O)(BQEN⁺)(NCCH₃)³⁺ with an iron(IV)-oxo group coupled to a ligand radical. As both doublet and quartet spin states represent the same orbital occupation, namely $\pi^*_{xy}{}^2 \pi^*_{xz}{}^1 \pi^*_{yz}{}^1 \pi^*_{\text{BQEN}}{}^1$, we calculate them within 2 kcal mol $^{-1}$. This result is similar to the spin state energies of ferromagnetically versus antiferromagnetically coupled doublet and quartet spin states of Compound I of P450, where these spin states were also found to be within a couple of kcal mol $^{-1}$ from each other. Moreover, the energy gap was found to be sensitive to the local environment, including hydrogen bonding interactions to the oxidant as well as solvent effects.²⁴ Furthermore, these two spin states result in two-state-reactivity patterns with substrates on

competing spin-state surfaces.²⁵ Analogously to P450 Compound I, the iron(V)-oxo species is an excited state of the molecular ground state with configuration [Fe^{IV}(O)(BQEN⁺)(NCCH₃)³⁺. Geometrically $^{2,4}\mathbf{2}$ has metal-ligand bond lengths close to those found for $^{3,5}\mathbf{1}$, which also is an iron(IV)-oxo species.

Reactant complexes.

Subsequently, ethylbenzene (EB) was added to the model complexes to create a long-range reactant complex (**RC**) as this was one of the substrates used in the experimental study and we investigated the benzyl hydroxylation processes. The electronic features of $^{3,5}\mathbf{RC}_1$ or $^{3,5}[\text{Fe}(\text{O})(\text{BQEN})(\text{NCCH}_3)\text{---EB}]^{2+}$ and $^{2,4}\mathbf{RC}_2$ or $^{2,4}[\text{Fe}(\text{O})(\text{BQEN})(\text{NCCH}_3)\text{---EB}]^{3+}$ will be discussed prior to the investigation of the catalytic mechanism. Considering that computational modelling occasionally is sensitive to the choice of the density functional used as well as on environmental variables,²⁶ some thorough testing of the structures, spin-state energetics and electronic configurations of $^{3,5}\mathbf{RC}_1$ and $^{2,4}\mathbf{RC}_2$ using a selection of density functional methods and procedures was carried out. Thus, we performed geometry optimizations of all complexes in the gas-phase at UB3LYP/BS1, but also did a full geometry optimization in a dielectric constant mimicking acetonitrile at UB3LYP/BS2 and finally a full geometry optimization in a dielectric constant at the UB3LYP-D3/BS2. In addition, single point calculations on the UB3LYP/BS2 optimized geometries using B3LYP with 15% HF exchange (B3LYP*), UB3LYP-D3 and OPBE were performed. Finally, single point calculations in the gas-phase with additional counter-ions or point charges included in the model at a distance of 15Å that neutralize the chemical systems were carried out.

Table 1 presents the optimized Fe–O distance and spin-state energies as obtained using these different DFT models and methods. As can be seen all methods, models and optimization techniques give the same spin state ordering, but a certain degree of variation in the relative energies is observed typical for DFT calculated iron complexes.²⁶ In all cases $^{3,5}\mathbf{RC}_1$ and $^{2,4}\mathbf{RC}_2$ are characterized as [Fe^{IV}(O)(BQEN)(NCCH₃)---EB]²⁺ with orbital occupation $\pi^*_{xy}{}^2 \pi^*_{xz}{}^1 \pi^*_{yz}{}^1$ and $\pi^*_{xy}{}^1 \pi^*_{xz}{}^1 \pi^*_{yz}{}^1 \sigma^*_{x^2-y^2}{}^1$, respectively, in agreement with what was found for structure $^{3,5}\mathbf{1}$ above. Regardless of the method and whether the optimization is done in the gas-phase or in solvent, a triplet spin ground state that is well separated from the quintet spin state by 2.4 – 10.3 kcal mol $^{-1}$ is found. Although this appears to be a large variation in spin state energies, actually for transition metal complexes, and, in particular iron(IV)-oxo complexes a strong variation of the ordering and relative energies is normal in DFT upon changing the density functional method or environmental effects.²⁷ Nevertheless, all methods give a triplet spin ground state in support of experimental studies.¹⁷

Table 1. Spin state energies and optimized geometries of reactant complexes as calculated with various DFT methods.

Structure	$r_{\text{FeO}}^{a,b}$	$r_{\text{FeO}}^{b,c}$	$r_{\text{FeO}}^{b,e}$	$\Delta E + \text{ZPE}$						
				UB3LYP	UB3LYP	UB3LYP-D3	UB3LYP-D3	UB3LYP	UB3LYP*	OPBE
				Gas ^{a,d}	Solv ^{c,d}	Solv ^{c,d}	Solv ^{d,e}	PC ^{c,f}	Solv ^{c,d}	Solv ^{c,d}
³ RC ₁	1.656	1.633	1.657	0.0	0.0	0.0	0.0	0.0	0.0	0.0
⁵ RC ₁	1.653	1.627	1.653	10.3	2.5	7.4	8.2	8.7	6.0	2.4
² RC ₂	1.664	1.638	1.656	0.0	0.0	0.0	0.0	0.0	0.0	0.0
⁴ RC ₂	1.664	1.631	1.653	0.6	-3.6	10.0	8.4	10.0	6.9	3.8

^a UB3LYP/BS1 geometry optimization in the gas-phase. ^b Values in Å. ^c UB3LYP/BS2 geometry optimization in solvent. ^d $\Delta E + \text{ZPE}$ value with energies at BS2 level of theory in kcal mol⁻¹. ^e UB3LYP-D3/BS2 geometry optimization in solvent. ^f Structure with added point charges that neutralize the system at 15 Å.

The situation is dramatically changed when ^{2,4}RC₂ is investigated with these methods and models. Whereas ^{2,4}2^{*} was found as the electronic ground state with configuration [Fe^{IV}(O)(BQEN⁺)(NCCH₃)³⁺] with two unpaired π^* electrons coupled to a radical on the ligand, by contrast, in ^{2,4}RC₂ we find yet another electronic configuration with two unpaired π^* electrons that are coupled to an ethylbenzene radical, i.e. orbital occupation $\pi_{xy}^{*2} \pi_{xz}^{*1} \pi_{yz}^{*1} \pi_{\text{BQEN}}^{*2} \pi_{\text{EB}}^{*1}$, where the latter orbital is a singly occupied π -orbital on ethylbenzene. Therefore, addition of an ethylbenzene molecule to ^{2,4}2^{*} results in an intermolecular electron transfer from the substrate into the π_{BQEN}^* orbital of the oxidant and the creation of a complex [Fe^{IV}(O)(BQEN)(NCCH₃)²⁺---EB⁺]. This happens regardless of the method and whether gas-phase or solvent models are used. It implies that [Fe^{IV}(O)(BQEN⁺)(NCCH₃)³⁺] is a strong oxidant and can abstract electrons from substrates readily. Most probably this is caused by its extremely large electron affinity, *vide supra*.

Note that outer-sphere electron transfer upon approach of a substrate onto a metal-oxo species has been calculated before on metal-porphyrins,^{28,29} including a potential intermediate of nitric oxide synthase, where the arginine substrate was found to donate an electron to an iron(IV)-oxo heme cation radical species quickly. Furthermore, approach of a Zn²⁺ ion onto a high-valent manganese(V)-oxo corrolazine also led to the formation of a manganese(IV)-oxo corrolazine cation radical through valence tautomerization.²⁹ Finally, studies on the comparative electronic features of the iron(IV)-oxo heme species of cytochrome *c* peroxidase (CcP) versus ascorbate peroxidase implicated differences in electronic configuration as a result of a bound cation at a distance of 15 Å from the heme. DFT modelling on Compound I of CcP tested the effect of a point charge with magnitude $Q = -1/+1$ on the electronic configuration.³⁰ It was found that a charge of $Q = +1$ gave an electronic state [Fe^{IV}(O)(heme⁺)---Trp₁₉₁], whereas a value of

$Q = -1$ resulted in an alternative state corresponding to [Fe^{IV}(O)(heme)---Trp₁₉₁⁺]. These studies have shown that seemingly small external (but long-range) perturbations can have a major impact on the electronic configuration of the oxidant and consequently on its ability to react with substrates. However, for nonheme metal-oxo species this would be the first example of outer-sphere electron transfer upon substrate approach and is likely caused by the large electron affinity of the ligand. In the following we will describe whether the change in electronic configuration is beneficial or disadvantageous to the catalysis.

Ethylbenzene hydroxylation by 1 and 2.

Subsequently, the benzyl hydroxylation of ethylbenzene by ^{3,5}RC₁ and ^{2,4}RC₂ was calculated. Fig 3 displays the calculated reaction mechanism with optimized geometries of the rate determining transition states of the reaction starting from ^{3,5}RC₁. We calculate a stepwise mechanism with an initial hydrogen atom abstraction from the benzyl position of ethylbenzene via a transition state (**TS**_{HA}) to form a radical intermediate (**I**) followed by hydroxyl rebound via a transition state (**TS**_{reb}) to form alcohol products (**P**). In all cases the hydrogen atom abstraction is rate determining and the rebound barriers are small or negligible, so that we will focus on **TS**_{HA} pathway only here. Full details of the rest of the mechanism are given in the Supporting Information. In the gas phase very little energy difference between hydrogen atom abstraction from the *pro-S* versus *pro-R* site of the benzyl position of ethylbenzene by iron(IV)-oxo complexes was found. Recent computational studies on *S*-mandalate synthase showed that the shape and size of the substrate binding pocket determines whether the *pro-R* or *pro-S* hydrogen atom can be abstracted.³¹ Indeed, site-selective mutations confirmed the computationally proposed hypothesis.

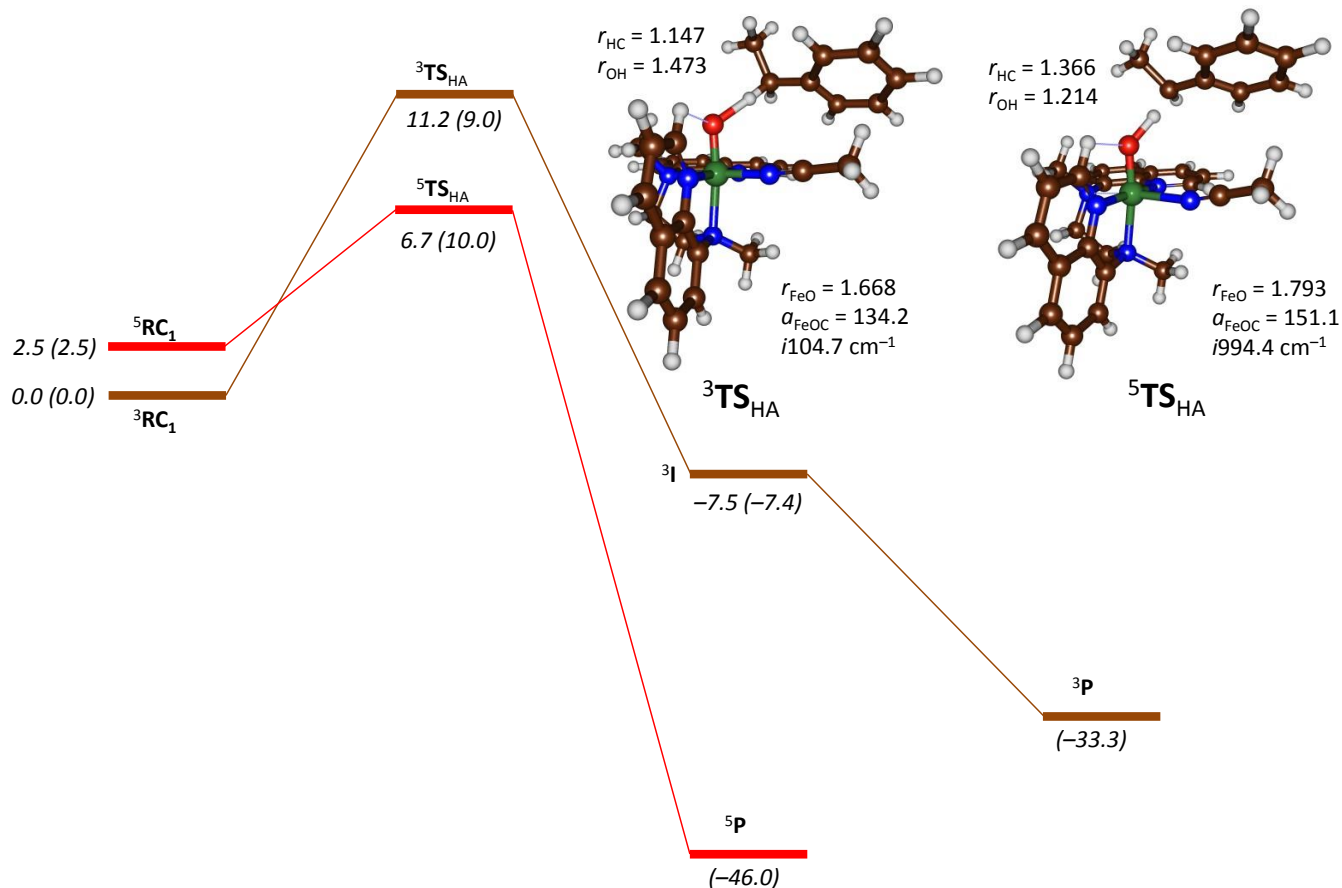


Fig 3. DFT calculated potential energy profile for the hydrogen atom abstraction from EB by ^{3,5}IB with energies given in kcal mol⁻¹. Also shown are optimized UB3LYP/BS2(solvent) geometries of ^{3,5}TS_{HA} with bond lengths in angstroms, angles in degrees and the imaginary frequency in wave numbers. Relative energies represent ΔE+ZPE+E_{solv} values obtained after a full geometry optimization in solvent at UB3LYP/BS2 (out of parenthesis) or at UB3LYP/BS2//UB3LYP/BS1 level of theory on a gas-phase optimized geometry.

Geometrically, the ^{3,5}TS_{HA} structures are quite distinct due to differences in electron transfer processes that happen in these transition states. In the triplet spin state the hydrogen atom transfer is accompanied with electron transfer from the substrate into the π*_{xz} orbital and hence the substrate attacks under an angle (α_{FeOC} = 134.2°) to get ideal orbital overlap between donor and acceptor orbitals.³² In the quintet spin state the hydrogen atom abstraction is accompanied with electron transfer from substrate into the vacant σ*_{z2} orbital and hence the substrate attacks from the top with considerably larger FeOC angles than found in the triplet spin state (α_{FeOC} = 151.1°), which gives an iron(III)-hydroxo complex with fully exchange coupled metal 3d system with five singly occupied orbitals that is anti-ferromagnetically coupled to a benzyl radical: ⁵I has electronic configuration π*_{xy}¹ π*_{xz}¹ π*_{yz}¹ σ*_{x2-y2}¹ σ*_{z2}¹ π_{EB}¹. This exchange stabilization makes ⁵I considerably lower in energy than the corresponding triplet spin complex. As a consequence, ⁵TS_{HA} is stabilized over ³TS_{HA}, although dispersion corrections make them almost degenerate.

Nevertheless, the barrier heights on both spin state surfaces are small and implicate an efficient hydrogen atom abstraction process in agreement with experiment.⁹ When the enthalpy values from Fig 3 are converted to a free energy of activation, a value of ΔG_{solv} = 10.8 kcal mol⁻¹ on the triplet spin state surface is found, which is in reasonable agreement with the experimentally reported free energy of activation of Nam et al.⁹

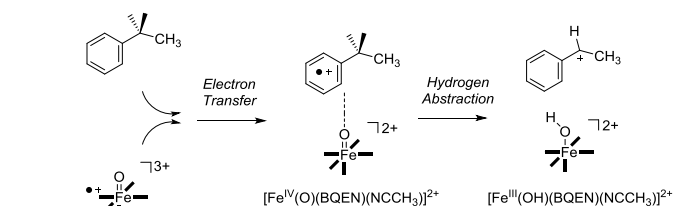
The experimental studies on ethylbenzene hydroxylation by RC₁ were found to proceed with a kinetic isotope effect (KIE) of 10 for the replacement of hydrogen atoms by deuterium in the substrate. To estimate the isotope effects for replacement of the transferrable hydrogen atom by deuterium in the reaction passing ³TS_{HA} we used the Eyring and Wigner models (see Methods section) to estimate the KIE. Values of KIE_E and KIE_W of 4.9 and 5.4 were obtained, whereas these values increased unto 5.1 and 5.7, respectively when the fully deuterated substrate was used. Our calculated isotope effect is, therefore, predicts the same trends as experiment.

Discussion

Our DFT calculations on $^{3,5}\mathbf{1}$ and $^{2,4}\mathbf{2}'$ reported above show that both systems are in the iron(IV) oxidation state and the oxidation of $\mathbf{2}'$ does not oxidize the metal to iron(VI) but rather keeps it at iron(IV) due to electron release from the BQEN macrocycle rather than the metal. Therefore, although $\mathbf{2}'$ is perceived as an iron(V)-oxo species, it actually is an iron(IV)-oxo with BQEN cation radical. Moreover, the DFT calculations reported in this work show that approach of a substrate, e.g. ethylbenzene, onto $^{4,2}\mathbf{2}'$, leads to a long-range electron transfer upon formation of the reactant complex $^{4,2}\mathbf{RC}_2$: $^3[\text{Fe}^{\text{IV}}(\text{O})(\text{BQEN})(\text{NCCH}_3)]^{2+} \cdots \text{EB}^{+\bullet}$, Scheme 2. The subsequent hydrogen atom abstraction then gives an iron(III)-hydroxo complexes and a $\text{C}_6\text{H}_5\text{CH}^+\text{CH}_3$ cation.

In previous studies, we showed that the driving force of a hydrogen atom abstraction correlates linearly with the free energy of activation.^{24d,27c,33} Therefore, to understand the thermodynamics and kinetics of the reaction mechanisms reported in Figs 2 and 3 above, we did a detailed analysis of the individual thermodynamic reaction steps for electron and hydrogen atom transfer processes, which are summarized in Fig 5. Panel (a) in Fig 5 starts on the top left with $\mathbf{2}'$ and the reaction to the right reflects a one-electron abstraction to form $\mathbf{31}$ and the subsequent one-electron abstraction to form $[\text{Fe}^{\text{III}}(\text{O})(\text{BQEN})(\text{NCCH}_3)]^+$. The vertical arrows reflect the hydrogen atom abstraction processes from both $\mathbf{2}'$ and $\mathbf{31}$.

Thermodynamically, the energy for these reactions is associated with the bond dissociation energy of the O–H bond in the metal-hydroxo complex to revert back into the iron-oxo and an isolated H-atom, as defined as BDE_{OH} . The calculated BDE_{OH} values for $\mathbf{2}'$ and $\mathbf{31}$ are virtually the same in the gas phase, which is not surprising as both complexes are iron(IV)-oxo intermediates. Therefore, geometrically very little differences in the hydrogen atom abstraction reactions will be obtained. The energy gap between the two BDE_{OH} values widens to 10.2 kcal mol⁻¹ in favour of $\mathbf{2}'$ when solvent, thermal and entropical corrections to the energy are included.



Scheme 2. Calculated reaction mechanism for $\mathbf{2}$ with oxidation states of critical intermediates identified.

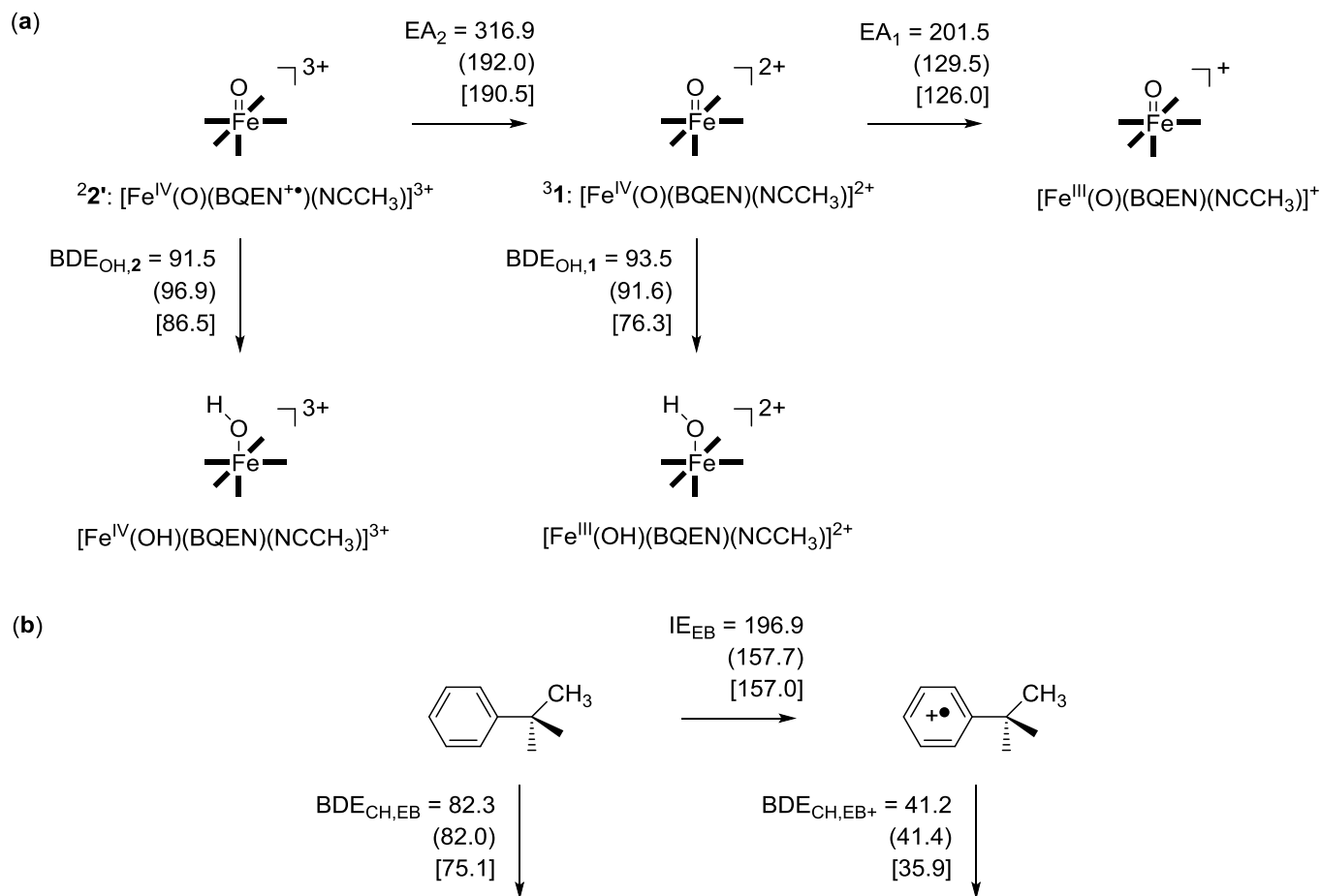


Fig 5. (a) Thermodynamic reaction pathways for electron and hydrogen atom abstraction by $\mathbf{1}$ and $\mathbf{2}$. (b) Thermodynamic reaction pathways for electron and hydrogen atom abstraction by EB. All data obtained from a geometry optimization at UB3LYP/BS2. Data (in kcal mol⁻¹) reported are $\Delta E + \text{ZPE}$ in the gas-phase ($\Delta E + \text{ZPE}$ in solvent) [ΔG in solvent].

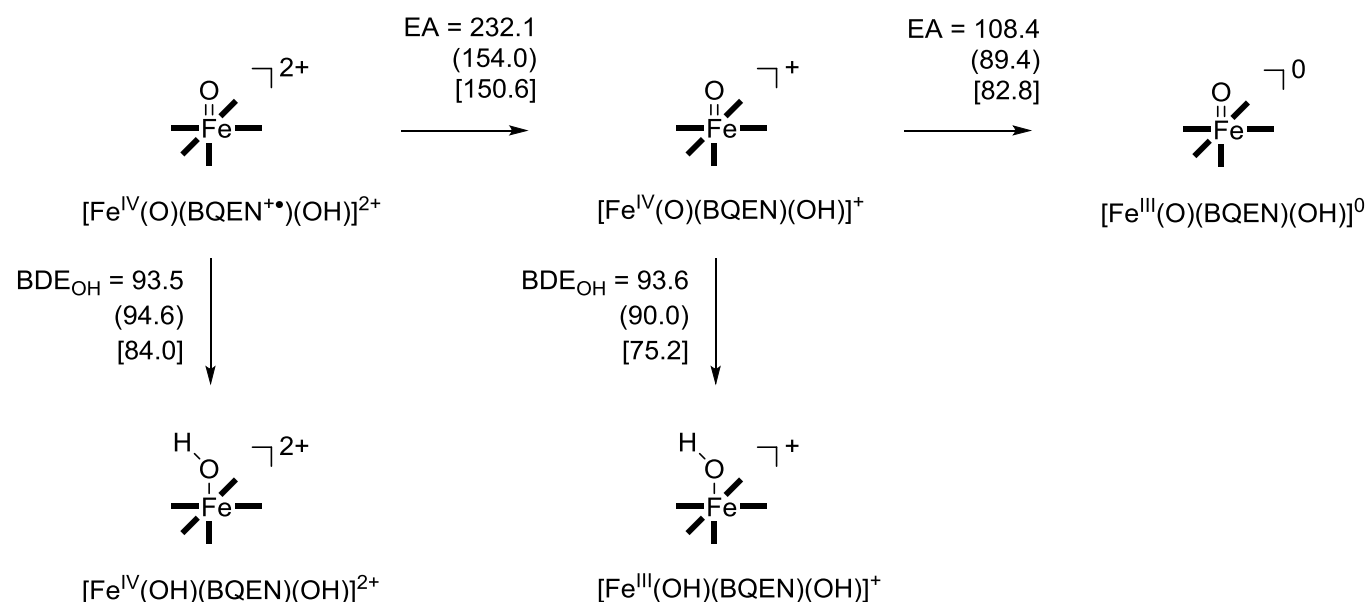


Fig 6. Thermodynamic reaction pathways for electron and hydrogen atom abstraction by $[\text{Fe}(\text{O})(\text{BQEN})(\text{OH})]^{2+}$ and $[\text{Fe}(\text{O})(\text{BQEN})(\text{OH})]^{+}$. All data obtained from a geometry optimization at UB3LYP/BS2. Data (in kcal mol^{-1}) reported are $\Delta E + \text{ZPE}$ in the gas-phase ($\Delta E + \text{ZPE}$ in solvent) [ΔG in solvent].

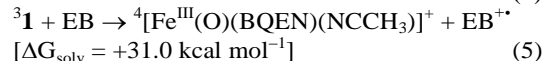
In the case of BDE_{OH} , solvent corrections stabilizes the value of $2'$ over 1 by $7.3 \text{ kcal mol}^{-1}$, whereas thermal and entropic corrections add a further $4.9 \text{ kcal mol}^{-1}$. These BDE_{OH} values, therefore, would predict higher reactivity of $2'$ over 31 in solvent for hydrogen atom abstraction reactions.

The major differences between 1 and $2'$, however, are related to their electron affinities or reduction potentials. Thus, $2'$ has a large electron affinity (EA_2) of $316.9 \text{ kcal mol}^{-1}$ in the gas-phase and $\Delta G_{\text{solv}} = 190.5 \text{ kcal mol}^{-1}$. It is worth noting that for all calculations we find almost equal values for $\Delta E + \text{ZPE} + E_{\text{solv}}$ and ΔG_{solv} , therefore, entropic and thermal corrections to the solvent corrected enthalpies have a negligible effect on the individual reactions studied. The electron affinity of $2'$ is considerably larger than that found for 31 , where values of $\text{EA}_1 = 201.5 \text{ kcal mol}^{-1}$ in the gas-phase and $\Delta G_{\text{solv}} = 126.0 \text{ kcal mol}^{-1}$ are found. Consequently, $2'$ has a $\Delta G_{\text{solv}} = 63.5 \text{ kcal mol}^{-1}$ larger electron affinity than 31 and will be more susceptible to react by electron abstraction from substrates.

For completeness we also include in Fig 6 the thermodynamics for ethylbenzene substrate for removal of an electron and the C–H bond strengths of the benzyl group of ethylbenzene and ethylbenzene cation radical. As already mentioned above ethylbenzene cation radical has a considerably weakened C–H bond strength of $\Delta G_{\text{solv}} = 35.9 \text{ kcal mol}^{-1}$ as compared to EB. Consequently, hydrogen atom abstraction from $\text{EB}^{+\bullet}$ will have a low barrier.

To find out whether a reaction of $2'$ and 31 with EB would lead to a large thermodynamic driving force for electron transfer, the free energy in solvent for the reactions given in Eqs 4 and 5 was calculated. Thus, the electron transfer from EB

to $2'$ is calculated to be exergonic by $33.5 \text{ kcal mol}^{-1}$, whereas the one originating from 31 is endergonic by $31.0 \text{ kcal mol}^{-1}$ instead. These two reactions implicate that in a collision between $2'$ and EB the driving force will trigger an electron abstraction from EB, whereas that will not be the case in a collision between 31 and EB. The large EA_2 value will, therefore, lead to a large driving force for electron transfer from suitable substrates including ethylbenzene to $2'$. Moreover, the thermodynamic reaction pathways given in Fig 5 give further evidence of a likely electron transfer between EB and $2'$.



Despite the fact that the BDE_{OH} values of 1 and $2'$ are virtually the same, actually at the free energy level with solvent included they are separated by about 10 kcal mol^{-1} . However, much more dramatic differences in the electron affinity of both complexes is found. Thus, the bond dissociation energy to break the A–H bond (BDE_{AH}) – or hydrogen atom abstraction ability of compound A – can be split into an individual electron and proton transfer via Eq 6, whereby ΔG_{acid} the acidity of the weak acid AH represents, EA_A is the electron affinity of A, and IE_H the ionization energy of a H-atom. The experimentally reported value of IE_H is 13.598 eV .³⁵



Using the data from Fig 5 and the known IE_H value we calculate a ΔG_{acid} of $590.5 \text{ kcal mol}^{-1}$ for $[\text{Fe}^{\text{IV}}(\text{OH})(\text{BQEN})(\text{NCCH}_3)]^{3+}$, whereas proton transfer to **1** gives the complex $[\text{Fe}^{\text{III}}(\text{OH})(\text{BQEN})(\text{NCCH}_3)]^{2+}$ with $\Delta G_{acid} = 515.9 \text{ kcal mol}^{-1}$. The large difference between EA_2 and EA_1 , therefore, has a direct impact on the acidity of the iron(III)-hydroxo group and makes it considerably more acidic. The origin of the difference in electron affinity of **1** and **2'** is due to difference in electron transfer processes. Upon reduction of **2'** an electron is transferred into the low-lying π^*_{BQEN} orbital to form a triplet spin $\pi^*_{xy}{}^2 \pi^*_{xz}{}^1 \pi^*_{yz}{}^1 \pi^*_{\text{BQEN}}{}^2$ configuration. On the other hand, reduction of **31** leads to filling of the virtual σ^*_{z2} orbital with a single electron. As the σ^*_{z2} orbital is significantly higher in energy than the π^*_{BQEN} orbital this means the reduction of **1** will incur a much smaller electron affinity than adding an electron to π^*_{BQEN} , which is indeed what is found in Fig 5.

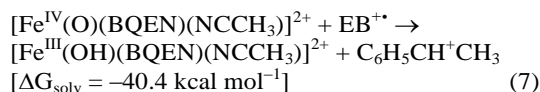
To find out whether the *cis*-ligand of the metal-oxo group affects the EA and ΔG_{acid} values, we did a further set of calculations on the electron and hydrogen atom transfer reactions for complexes $[\text{Fe}^{\text{IV}}(\text{O})(\text{BQEN}^+)(\text{OH})]^{2+}$ and $[\text{Fe}^{\text{IV}}(\text{O})(\text{BQEN})(\text{OH})]^+$, i.e. complexes **2'** and **1** that have the acetonitrile ligand replaced by OH^- . We should note here that replacement of the acetonitrile equatorial ligand by hydroxide does not change the spin state ordering and electronic configuration and these complexes are characterized like **2'** and **1** above. Fig 6 displays the thermodynamic reaction pathways for $[\text{Fe}^{\text{IV}}(\text{O})(\text{BQEN}^+)(\text{OH})]^{2+}$ and $[\text{Fe}^{\text{IV}}(\text{O})(\text{BQEN})(\text{OH})]^+$. Firstly, very little effect of replacing the acetonitrile with hydroxide is found on the BDE_{OH} values of the complexes. For $[\text{Fe}^{\text{IV}}(\text{O})(\text{BQEN})(\text{OH})]^{2+}$ we find a BDE_{OH} value of $\Delta G_{\text{solv}} = 84.0 \text{ kcal mol}^{-1}$, whereas its one-electron reduced counterpart has a $\Delta G_{\text{solv}} = 75.2 \text{ kcal mol}^{-1}$. These values are within $2.5 \text{ kcal mol}^{-1}$ from those obtained with an acetonitrile molecule in the *cis*-position. The situation, however, changes dramatically for the electron affinities and acidity values of the complexes when the acetonitrile ligand is replaced by hydroxide. Thus, $[\text{Fe}^{\text{IV}}(\text{O})(\text{BQEN}^+)(\text{OH})]^{2+}$ has an electron affinity of $\Delta G_{\text{solv}} = 150.6 \text{ kcal mol}^{-1}$, whereas the much lower value of $82.8 \text{ kcal mol}^{-1}$ is found for $[\text{Fe}^{\text{IV}}(\text{O})(\text{BQEN})(\text{OH})]^+$. These lowered electron affinities with respect to complexes **2'** and **1** also mean reduced acidity of the protonated complexes, for which we find values of 548.2 and $471.6 \text{ kcal mol}^{-1}$, respectively.

In addition, a reaction of $[\text{Fe}^{\text{IV}}(\text{O})(\text{BQEN}^+)(\text{OH})]^{2+}$ with ethylbenzene is calculated to give an endergonic electron transfer of $6.4 \text{ kcal mol}^{-1}$ using the data given in Figs 5 and 6. Therefore, replacing the acetonitrile equatorial ligand in complex **2'** with an anion such as a hydroxide will affect the stability and reactivity of the complex and will prevent a long-range electron transfer with substrates like ethylbenzene. The electron transfer from ethylbenzene to $[\text{Fe}^{\text{IV}}(\text{O})(\text{BQEN})(\text{OH})]^+$ is calculated to be even more endergonic ($\Delta G_{\text{solv}} = 74.2 \text{ kcal mol}^{-1}$) and consequently is not likely to happen.

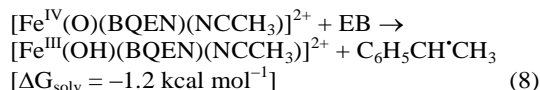
In summary, we establish reasons for the large thermodynamic driving force for electron transfer from ethylbenzene to **2'** as originating from a high electron affinity of the oxidant of $\Delta G_{\text{solv}} = 190.5 \text{ kcal mol}^{-1}$. This implies that the electron transfer to the approaching substrate could be spontaneous for substrates with an ionization potential below $190.5 \text{ kcal mol}^{-1}$ or 8.26 eV . Although, we calculate an ionization energy of 8.54 eV in the gas phase actually in solution the value drops to $\Delta G_{\text{solv}} = 6.81 \text{ eV}$. Therefore, in solution the ionization potential of ethylbenzene is sufficiently

low to incur a long-range electron transfer to the oxidant and create ${}^3[\text{Fe}^{\text{IV}}(\text{O})(\text{BQEN})(\text{NCCH}_3)]^{2+} \text{---} {}^2\text{EB}^{\bullet+}$.

Finally, the thermodynamics values of Figs 6 and 7 also enable us to predict the hydrogen atom transfer driving force in complexes **RC**₂ and **RC**₁. As described above, **RC**₂ undergoes a long-range electron transfer and converts to $[\text{Fe}^{\text{IV}}(\text{O})(\text{BQEN})(\text{NCCH}_3)]^{2+}$ and $\text{EB}^{\bullet+}$. This complex reacts via hydrogen atom transfer via Eq 7 with a free energy change of $-40.4 \text{ kcal mol}^{-1}$. The DFT calculations for this process, see Electronic Supporting Information, implicated a free energy change of $\Delta G_{\text{solv}} = -42.4 \text{ kcal mol}^{-1}$ for the formation of the radical intermediate **2I**, and therefore its calculated value is in good agreement with the value estimated from our thermodynamic cycles.



By contrast, if we do the same for complex **RC**₁ and take the difference in free energy between the BDE_{CH} and BDE_{OH} values of oxidant and substrate, we find an almost thermoneutral hydrogen atom abstraction reaction, Eq 8. Indeed, the DFT calculations above predict a radical intermediate with exergonicity of $6.9 \text{ kcal mol}^{-1}$ with respect to the reactant complex in good agreement with the thermodynamically estimated value.



To test whether the electron transfer observed here in our reactant complexes is a general feature that could be found in alternative iron(V)-oxo complexes as well, we decided to also investigate the well-studied $[\text{Fe}(\text{O})(\text{TPA})(\text{OH})]^{2+}$, TPA = tris-(2-pyridylmethyl)amine, system of Costas and co-workers.^{10b} Previously, $[\text{Fe}(\text{O})(\text{TPA})(\text{X})]^{2+}$ with X = halide or OH^- has been used in studies of the *cis*-effect on substrate activation by metal-oxo species, but also as a model for non-heme iron halogenases. Technically the $[\text{Fe}(\text{O})(\text{TPA})(\text{OH})]^{2+}$ is an iron(V)-oxo complex as indeed confirmed by DFT calculations.³⁶ The question, of course, arises whether the oxidation state of the complex stays in the iron(V) state upon approach of an ethylbenzene molecule. Thus, we optimized the reactant complex $[\text{Fe}(\text{O})(\text{TPA})(\text{OH})\text{---}\text{EB}]^{2+}$ in the doublet and quartet spin states at UB3LYP-D3/BS2 level of theory and show the structures and group spin densities of the complexes alongside those of ${}^{4,2}\text{RC}_2$ in Fig 7.

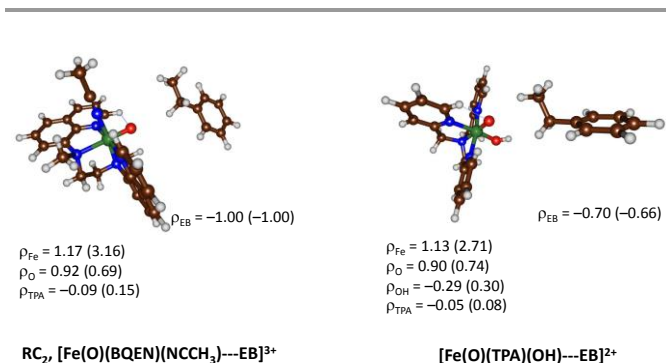


Fig 7. Group spin densities of ${}^{4,2}\text{RC}_2$ and $[\text{Fe}(\text{O})(\text{TPA})(\text{OH})\text{---}\text{EB}]^{2+}$ as calculated with UB3LYP/BS2 in solvent. High-spin data in parenthesis.

The results in Fig 7 show that upon approach of an ethylbenzene molecule to an iron(V)-oxo center, a long-range electron transfer takes place from substrate to oxidant. Therefore, the group spin densities of $^{2,4}\text{RC}_2$ and $[\text{Fe}(\text{O})(\text{TPA})(\text{OH})\text{---EB}]^{2+}$ both refer to an iron(IV)-oxo complex with a nearby $\text{EB}^{\cdot+}$ ion. Both complexes have a doublet spin state with $\pi_{xy}^{*2} \pi_{xz}^{*1} \pi_{yz}^{*1} \pi_{\text{EB}}^1$ configuration, i.e. a triplet spin iron(IV)-oxo complex with a nearby doublet cation radical ethylbenzene. By contrast the quartet spin state configurations of these complexes have orbital occupation $\pi_{xy}^{*2} \pi_{xz}^{*1} \pi_{yz}^{*1} \sigma_{z2}^{*1} \pi_{\text{EB}}^1$ configuration with the ethylbenzene radical anti-ferromagnetically coupled to three unpaired electrons on the iron(IV)-oxo complex. Note that without ethylbenzene present the $[\text{Fe}(\text{O})(\text{TPA})(\text{OH})]^{2+}$ complex converges to an iron(V)-oxo species and no ligand radical is found. The TPA ligand, therefore, has much lower lying molecular orbitals than a BQEN ligand system and as a result the π_{BQEN} orbitals become competitive with the π_{xz}^*/π_{yz}^* orbitals on the FeO group. As a result of this $[\text{Fe}(\text{O})(\text{BQEN})(\text{NCCH}_3)]^{3+}$ has an electronic configuration representing an iron(IV)-oxo coupled to a ligand radical, whereas $[\text{Fe}(\text{O})(\text{TPA})(\text{OH})]^{2+}$ is an iron(V)-oxo species.

Conclusions

In summary, we present here the first comparative study on the reactivity patterns of nonheme iron(IV)-oxo versus iron(V)-oxo intermediates. Upon approach of the substrate to the iron(IV)-oxo ligand cation radical it abstracts an electron from substrate readily, and thereby creates an iron(IV)-oxo ligand cation radical species. The perceived reactivity of the iron(V)-oxo species, therefore, is due to activity of the iron(IV)-oxo ligand cation radical instead. We also show that oxidation of ethylbenzene weakens the C–H bond strength of the substrate and thereby lowers the hydrogen atom abstraction barriers and leads to higher reactivity. This is an example of how outer-sphere (long-range) electron transfer can change the C–H bond strength of the substrate so that a more efficient H-transfer becomes possible. The outer-sphere electron transfer may be a common feature in transition metal catalysis, but further research will be needed to find more examples of this type of reactivity patterns.

Acknowledgements

SdV thanks the Royal Society for an International Exchanges with Korea grant. The National Service of Computational Chemistry Software (NSCCS) is acknowledged for cpu time. DK acknowledges Department of Science and Technology (New Delhi) for a Ramanujan Fellowship. The research at EWU was supported by NRF of Korea through CRI (NRF-2012R1A3A2048842) and GRL (NRF-2010-00353).

Notes and references

^a Manchester Institute of Biotechnology and School of Chemical Engineering and Analytical Science, the University of Manchester, 131 Princess Street, Manchester M1 7DN, United Kingdom. Fax: +44 1613065201; Tel: +44 1613064882; E-mail: sam.devisser@manchester.ac.uk

^b Department of Applied Physics, School for Physical Sciences, Babasaheb Bhimrao Ambedkar University, Vidya Vihar, Rai Bareilly Road, Lucknow 226 025, India. E-mail: dkclcre@yahoo.com

^c Department of Chemistry and Nano Science, Ewha Womans University, Seoul 120-750, Korea. E-mail: wynam@ewha.ac.kr

[†] Footnotes should appear here. These might include comments relevant to but not central to the matter under discussion, limited experimental and spectral data, and crystallographic data.

Electronic Supplementary Information (ESI) available: Tables with absolute and relative energies as well as group spin densities and charges is provided as electronic supporting information. See DOI: 10.1039/b000000x/

- E. I. Solomon, T. C. Brunold, M. I. Davis, J. N. Kemsley, S.-K. Lee, N. Lehnert, F. Neese, A. J. Skulan, Y.-S. Yang and J. Zhou, *Chem. Rev.*, 2000, **100**, 235; b) T. D. H. Bugg and S. Ramaswamy, *Curr. Opin. Chem. Biol.*, 2008, **12**, 134; c) M. J. Ryle and R. P. Hausinger, *Curr. Opin. Chem. Biol.*, 2002, **6**, 193; d) Y. Mishina, E. M. Duguid and C. He, *Chem. Rev.*, 2006, **106**, 215; e) S. P. de Visser and D. Kumar (Eds.) *Iron-containing enzymes: Versatile catalysts of hydroxylation reactions in nature*. RSC Publishing, Cambridge (UK), 2011; f) P. He and G. R. Moran, *Curr. Opin. Chem. Biol.*, 2009, **13**, 443; g) D. Buongiorno and G. D. Straganz, *Coord. Chem. Rev.*, 2013, **257**, 541.
 - M. Costas, M. P. Mehn, M. P. Jensen and L. Que Jr., *Chem. Rev.*, 2004, **104**, 939; b) S. V. Kryatov, E. V. Rybak-Akimova and S. Schindler, *Chem. Rev.*, 2005, **105**, 2175; c) M. M. Abu-Omar, A. Loaiza and N. Hontzeas, *Chem. Rev.*, 2005, **105**, 2227; d) R. van Eldik, *Coord. Chem. Rev.*, 2007, **251**, 1649; e) P. C. A. Bruijninx, G. van Koten and R. J. M. Klein Gebbink, *Chem. Soc. Rev.*, 2008, **37**, 2716; f) S. P. de Visser, J.-U. Rohde, Y.-M. Lee, J. Cho and W. Nam, *Coord. Chem. Rev.*, 2013, **257**, 381; g) W. Nam, Y.-M. Lee and S. Fukuzumi, *Acc. Chem. Res.*, 2014, **47**, 1146.
 - See, e.g., a) M. R. Bukowski, K. D. Koehntop, A. Stubna, E. L. Bominaar, J. A. Halfen, E. Münck, W. Nam and L. Que Jr., *Science*, 2005, **310**, 1000; b) J.-U. Rohde, J.-H. In, M. H. Lim, W. W. Brennessel, M. R. Bukowski, A. Stubna, E. Münck, W. Nam and L. Que Jr, *Science*, 2003, **299**, 1037; c) M. Martinho, F. Banse, J.-F. Bartoli, T. A. Mattioli, P. Battioni, P.; Horner, S. Bourcier and J.-J. Girerd, *Inorg. Chem.*, 2005, **44**, 9592; d) C. V. Sastri, M. S. Seo, M. J. Park, K. M. Kim and W. Nam, *Chem. Commun.*, 2005, 1405; e) F. T. De Oliveira, A. Chanda, D. Banerjee, X. Shan, S. Mondal, L. Que Jr, E. L. Bominaar, E. Münck and T. J. Collins, *Science*, 2007, **315**, 835; f) T. A. Jackson, J.-U. Rohde, M. S. Seo, C. V. Sastri, R. DeHont, A. Stubna, T. Ohta, T. Kitagawa, E. Münck, W. Nam and L. Que Jr, *J. Am. Chem. Soc.*, 2008, **130**, 12394.
 - K. Chen, M. Costas, J. Kim, A. K. Tipton and L. Que Jr, *J. Am. Chem. Soc.*, 2002, **124**, 3026; b) A. Company, L. Gómez, M. Güell, X. Ribas, J. M. Luis, L. Que Jr and M. Costas, *J. Am. Chem. Soc.*, 2007, **129**, 15766; c) R. Mas-Ballesté, M. Fujita and L. Que Jr, *Dalton Trans.*, 2008, 1828; d) P. Comba, M. Maurer and P. Vadivelu, *Inorg. Chem.*, 2009, **48**, 10348; e) A. Company, Y. Feng, M. Güell, X. Ribas, J. M. Luis, L. Que Jr and M. Costas, *Chem. Eur. J.*, 2009, **15**, 3359; f) I. Prat, J. S. Mathieson, M. Güell, X. Ribas, J. M. Luis, L. Cronin and M. Costas, *Nature Chem.*, 2011, **3**, 788.

- 5 a) K. Chen and L. Que Jr, *J. Am. Chem. Soc.*, 2001, **123**, 6327; b) A. D. Ryabov, *Adv. Inorg. Chem.*, 2013, **65**, 117.
- 6 a) A. Nielsen, F. B. Larsen, A. D. Bond and C. J. McKenzie, *Angew. Chem. Int. Ed.*, 2006, **45**, 1602; b) A. Lennartson and C. J. McKenzie, *Angew. Chem. Int. Ed.*, 2012, **51**, 6767.
- 7 S. H. Lee, J. H. Han, H. Kwak, S. J. Lee, E. Y. Lee, H. J. Kim, J. H. Lee, C. Bae, S. N. Lee, Y. Kim and C. Kim, *Chem. Eur. J.*, 2007, **13**, 9393.
- 8 S. Kundu, J. Van Kirk Thompson, A. D. Ryabov and T. J. Collins, *J. Am. Chem. Soc.*, 2011, **133**, 18546.
- 9 J. Yoon, S. A. Wilson, Y. K. Jang, M. S. Seo, K. Nehru, B. Hedman, K. O. Hodgson, E. Bill, E. I. Solomon and W. Nam, *Angew. Chem. Int. Ed.*, 2009, **48**, 1257.
- 10 a) *Jaguar*, version 7.9, Schrodinger, LLC, New York, NY, 2011; b) *Gaussian-09*, Revision C.01, Gaussian Inc., Wallingford CT, 2010.
- 11 a) A. D. Becke, *J. Chem. Phys.*, 1993, **98**, 5648; b) C. Lee, W. Yang and R. G. Parr, *Phys. Rev. B*, 1988, **37**, 785.
- 12 a) S. P. de Visser, *Angew. Chem. Int. Ed.*, 2006, **45**, 1790; b) D. Kumar, W. Thiel and S. P. de Visser, *J. Am. Chem. Soc.*, 2011, **133**, 3869.
- 13 S. Grimme, *J. Chem. Phys.*, 2006, **124**, 034108.
- 14 M. Reiher, O. Salomon and B. A. Hess, *Theor. Chem. Acc.*, 2001, **107**, 48.
- 15 N. C. Handy and A. J. Cohen, *Mol. Phys.*, 2001, **99**, 403; b) J. P. Perdew, K. Burke and M. Ernzerhof, *Phys. Rev. Lett.*, 1996, **77**, 3865.
- 16 S. P. de Visser, M. G. Quesne, B. Martin, P. Comba and U. Ryde, *Chem. Commun.*, 2014, **50**, 262.
- 17 a) P. J. Hay and W. R. Wadt, *J. Chem. Phys.*, 1985, **82**, 270; b) W. J. Hehre, R. Ditchfield and J. A. Pople, *J. Chem. Phys.*, 1972, **56**, 2257.
- 18 a) A. K. Vardhaman, C. V. Sastri, D. Kumar and S. P. de Visser, *Chem. Commun.*, 2011, **47**, 11044; b) A. K. Vardhaman, P. Barman, S. Kumar, C. V. Sastri, D. Kumar and S. P. de Visser, *Angew. Chem. Int. Ed.*, 2013, **52**, 12288; c) A. K. Vardhaman, P. Barman, S. Kumar, C. V. Sastri, D. Kumar and S. P. de Visser, *Chem. Commun.*, 2013, **49**, 10926.
- 19 a) S. P. de Visser, *Chem. Eur. J.*, 2006, **12**, 8168; b) D. J. Heyes, M. Sakuma, S. P. de Visser and N. S. Scrutton, *J. Biol. Chem.*, 2009, **284**, 3762.
- 20 D. Kumar, S. P. de Visser, P. K. Sharma, S. Cohen and S. Shaik, *J. Am. Chem. Soc.*, 2004, **126**, 1907.
- 21 a) D. Kumar, H. Hirao, L. Que Jr and S. Shaik, *J. Am. Chem. Soc.*, 2005, **127**, 8026; b) S. P. de Visser, *J. Am. Chem. Soc.*, 2006, **128**, 15809; c) S. Ye and F. Neese, *Proc. Natl. Acad. Sci. USA*, 2011, **108**, 1228.
- 22 a) M. T. Green, *J. Am. Chem. Soc.*, 1999, **121**, 7939; b) J. Rittler and M. T. Green, *Science*, 2010, **330**, 933; c) K. Yoshizawa, Y. Shiota and T. Yamabe, *J. Am. Chem. Soc.*, 1999, **121**, 147.
- 23 a) S. P. de Visser, *J. Am. Chem. Soc.*, 2006, **128**, 9813; b) L. Bernasconi and E.-J. Baerends, *Eur. J. Inorg. Chem.*, 2008, 1672; c) C. Y. Geng, S. Ye and F. Neese, *Angew. Chem. Int. Ed.*, 2010, **49**, 5717; d) S. Shaik, H. Chen and D. Janardanan, *Nature Chem.*, 2011, **3**, 19; e) P. Comba, M. Maurer and P. Vadivelu, *Inorg. Chem.*, 2009, **48**, 10389.
- 24 a) J. C. Schöneboom, H. Lin, N. Reuter, W. Thiel, S. Cohen, F. Ogliaro and S. Shaik, *J. Am. Chem. Soc.*, 2002, **124**, 8142; b) S. P. de Visser, S. Shaik, P. K. Sharma, D. Kumar and W. Thiel, *J. Am. Chem. Soc.*, 2003, **125**, 15779; c) S. P. de Visser, L. Tahsini and W. Nam, *Chem. Eur. J.*, 2009, **15**, 5577; d) D. Kumar, G. N. Sastry and S. P. de Visser, *Chem. Eur. J.*, 2011, **17**, 6196.
- 25 S. Shaik, H. Hirao and D. Kumar, *Nat. Prod. Rep.*, 2007, **24**, 533.
- 26 M. G. Quesne, R. Latifi, L. E. Gonzalez-Ovalle, D. Kumar and S. P. de Visser, *Chem. Eur. J.*, 2014, **20**, 435.
- 27 See, e.g., a) M. Güell, J. M. Luis, M. Solà and M. Swart, *J. Phys. Chem. A*, 2008, **112**, 6384; b) R. Latifi, M. A. Sainna, E. V. Rybak-Akimova and S. P. de Visser, *Chem. Eur. J.*, 2013, **19**, 4058; c) D. Kumar, R. Latifi, S. Kumar, E. V. Rybak-Akimova, M. A. Sainna and S. P. de Visser, *Inorg. Chem.*, 2013, **52**, 7968.
- 28 S. P. de Visser and L. S. Tan, *J. Am. Chem. Soc.*, 2008, **130**, 12961.
- 29 P. Leeladee, R. A. Baglia, K. A. Prokop, R. Latifi, S. P. de Visser and D. P. Goldberg, *J. Am. Chem. Soc.*, 2012, **134**, 10397.
- 30 S. P. de Visser, *J. Phys. Chem. A*, 2005, **109**, 11050.
- 31 S. M. Pratter, C. Konstantinovic, C. L. M. DiGiuro, E. Leitner, D. Kumar, S. P. de Visser, G. Grogan, G. D. Straganz, *Angew. Chem. Int. Ed.*, 2013, **52**, 9677.
- 32 S. Sahu, L. R. Widger, M. G. Quesne, S. P. de Visser, H. Matsumura, P. Moëgne-Loccoz, M. A. Sieglar and D. P. Goldberg, *J. Am. Chem. Soc.*, 2013, **135**, 10590.
- 33 R. Latifi, M. Bagherzadeh and S. P. de Visser, *Chem. Eur. J.*, 2009, **15**, 6651.
- 34 X. Wu, M. S. Seo, K. M. Davis, Y.-M. Lee, J. Chen, K.-B. Cho, Y. N. Pushkar and W. Nam, *J. Am. Chem. Soc.*, 2011, **133**, 20088.
- 35 S. G. Lias, In *Ionization Energy Evaluation in NIST Chemistry WebBook*, NIST Standard Reference Database Number 69: P. J. Linstrom and W. G. Mallard (Eds.) National Institute of Standards and Technology: Gaithersburg MD, June 2005; 20899 (<http://webbook.nist.gov>).
- 36 a) Y. Ma and P. B. Balbuena, *J. Phys. Chem. B*, 2007, **111**, 2711; b) P. Comba, G. Rajaraman and H. Rohwer, *Inorg. Chem.*, 2007, **46**, 3826; c) A. Bassan, M. R. A. Blomberg, P. E. M. Siegbahn and L. Que Jr, *J. Am. Chem. Soc.*, 2002, **124**, 11056; d) S. P. de Visser and W. Nam, *J. Phys. Chem. A*, 2008, **112**, 12887.

Table of Content Figure:

